Acid Denaturation of Recombinant Porcine Growth Hormone: Formation and Self-Association of Folding Intermediates†

Emma J. Parkinson,‡,§ Michael B. Morris,|| and Stan Bastiras*,‡

BresaGen Ltd., P.O. Box 259, Rundle Mall Adelaide, SA 5000, Australia, Department of Biochemistry, University of Adelaide, Adelaide, SA 5005, Australia, and Faculty of Pharmacy, University of Sydney, Sydney, NSW 2006, Australia

Received March 10, 2000; Revised Manuscript Received June 16, 2000

ABSTRACT: We have investigated the conformational changes incurred during the acid-induced unfolding and self-association of recombinant porcine growth hormone (pGH). Acidification (pH 8 to pH 2) of pGH resulted in intrinsic fluorescence, UV absorbance, and near-UV CD transitions centered at pH 4.10. At pH 2.0, a red shift in the fluorescence emission maximum of ∼3 nm and a 15% loss of the far-UV CD signal at 222 nm imply that the protein did not become extensively unfolded. Acidification in the presence of 4 M urea resulted in similar pH-dependent transitions. However, these occurred at a higher pH (∼5.2). At pH 2.0 + 4 M urea, an 8 nm red shift in the fluorescence emission maximum suggests that unfolding was greater than in the absence of urea. The presence of a prominent peak centered at 298 nm in the near-UV CD spectrum, which is absent without urea, signifies further differences in the intermediates generated at pH 2. Sedimentation equilibrium experiments in the analytical ultracentrifuge showed that native pGH and the partially unfolded intermediates reversibly self-associate. Self-association was strongly promoted at pH 2 while urea reduced self-association at both pH 8 and pH 2. These results demonstrate that acidification of pGH in the absence or presence of 4 M urea induced the formation of molten globule-like states with measurable differences in conformation. Similarities and differences in these structural conformations with respect to other growth hormones are discussed.

The detection of partially folded intermediate states, including molten globules, along a protein's folding pathway is crucial to understanding the principles of protein folding (*1*−*5*). Molten globules are intermediates in the folding pathway of many proteins (*6*) and can be bound to molecular chaperones (*7*). More recently, the involvement of folding intermediates in several human diseases has reiterated their importance (*8*, *9*). It is now apparent that molten globule folding intermediates cover a broad range of conformations and degrees of unfolding, subject to the solvent conditions employed (*3*, *10*−*13*). Despite these variations, the characteristics of molten globules include (i) a significant amount of nativelike secondary structure, (ii) a collapsed state with hydrodynamic properties more akin to the native state, (iii) a lack of well-defined tertiary structure, (iv) enhanced solvent exposure of hydrophobic surfaces, and (v) a less cooperative unfolding transition compared to that of the native state (*3*−*5*, *13*).

Molten globules have been observed frequently at low pH, where intramolecular charge repulsion appears to be an important driving force for partial protein unfolding. Recently, De Filippis et al. (*14*) showed that the acid-induced molten globule of a fully active mutant of human interleukin-6 is involved in the pathogenesis of inflammation. Hence, there is increasing evidence of pathophysiological roles for the acid-induced molten globule or folding intermediate.

Porcine growth hormone (pGH)[1] is a member of the class of large pituitary polypeptide hormones. It is a single-chain polypeptide containing 191 amino acids arranged to form an antiparallel four α-helix bundle (*15*). The tertiary structures of human growth hormone (hGH; *16*) and bovine growth hormone (bGH; *17*) are very similar to that of pGH. This is consistent with pGH sharing 91% and 68% primary sequence identity with bGH and hGH, respectively.

Previous studies on the acid-induced unfolding of bGH and hGH showed that an intermediate(s) is (are) formed at pH 2.0. However, the observed structural properties of these intermediates are different. At pH 2.0, bGH exhibits characteristics similar to those attributed to the molten globule: little or no tertiary structure and a 50% loss of secondary structure compared to the native protein (*18*, *19*). In contrast, acidification (pH 2.0) of hGH results in conformations that maintain close secondary and tertiary structural similarity to that of the native state. When subjected to Gdn-HCl-induced denaturation at pH 2.0, hGH was shown to form highly stabilized equilibrium intermediates (*20*).

In view of the differences observed for the acidification of bGH and hGH, this report characterizes the acid-induced unfolding of pGH and subsequent structural alterations. The

† This research was supported by an Australian Postgraduate Award (Industry) to E.J.P. and by a Ramaciotti Foundation grant to M.B.M.

* To whom correspondence should be addressed. Phone: +61-8-82342660. Fax: +61-8-82346268. E-mail: sbastiras@bresagen.com.au.

‡ BresaGen Ltd.

§ University of Adelaide.

|| University of Sydney.

[1] Abbreviations: *B*, second virial coefficient; bGH, bovine growth hormone (somatotropin); hGH, human growth hormone; I_{340}, relative fluorescence intensity at 340 nm; λ_{max}, wavelength of maximum emission; $M_{w,app}$, apparent point-average weight-average molecular weight; pGH, porcine growth hormone; SEK, sequential equal equilibrium constant self-association; ϵ_{290}, molar extinction coefficient at 290 nm; $[\theta]_{MRW}$, mean residue ellipticity; θ_{285}, mean residue ellipticity at 285 nm.

10.1021/bi0005658 CCC: $19.00
Published on Web 09/08/2000

acid-induced equilibrium denaturation was followed by various probes of tertiary (UV absorption spectroscopy, intrinsic fluorescence, and near-UV circular dichroism) and secondary (far-UV circular dichroism) structure. Changes in self-association were followed by size-exclusion chromatography and analytical ultracentrifugation. Our findings indicate that, at low pH ± 4 M urea, pGH forms intermediates with the characteristics of molten globules. The properties of these molten globules, including their self-association, differ in many respects to those observed for bGH and hGH under similar conditions.

EXPERIMENTAL PROCEDURES

Materials. Recombinant-derived methionyl-pGH was produced at BresaGen Ltd., Adelaide, Australia. A combination of N-terminal sequence analysis (Applied Biosystems, Inc., Model 470A protein sequencer), mass spectrometry (Perkin-Elmer SCI-EX API100), and SDS−PAGE was used to verify the identity and homogeneity of the product. Urea was ultrapure grade from Merck. All other chemicals were analytical grade. Superose 12 HR10/30 size-exclusion columns were from Pharmacia. Proteins used for molecular weight calibration of the Superose 12 column were purchased from Sigma.

Acid Denaturation Experiments. Solutions of pGH at final concentrations of 0.05, 0.22, and 0.5 mg/mL were prepared by dissolving lyophilized pGH at pH 8.0 in either a combination buffer (20 mM each of sodium acetate, sodium bicarbonate, MES, and Tris-HCl) or 100 mM sodium phosphate. Duplicate solutions were also prepared in the same buffer plus 4 M urea. Titrations were typically carried out by the careful addition of small aliquots of 1 M HCl with continual mixing. Following adjustment of pH, the samples were incubated for approximately 1 h at room temperature and centrifuged (12000*g*, 10 min). The protein concentration of the supernatant was checked by absorbance at 278 nm using an extinction coefficient of 15 714 M^{-1} cm^{-1} (*21*). All pH measurements during titrations were conducted at 25 ± 0.5 °C using an Activon Model 209 pH meter. Apparent midpoints of pH transitions were determined by fitting the data to a sigmoid curve function (*22*).

Intrinsic Fluorescence. Intrinsic fluorescence measurements were recorded at 25 °C on an Aminco Bowman AB-2 luminescence spectrometer. All fluorescence data were obtained using an excitation wavelength of 295 nm, slit widths of 4 nm for both monochromators, and a scan rate of 60 nm/min. Fluorescence intensities and maximum emission wavelengths (λ_{max}) were determined from emission spectra acquired in the range 310−400 nm and corrected for buffer contributions. The concentrations of pGH used were 0.05, 0.22, and 0.5 mg/mL.

UV Absorbance. UV absorbance measurements were recorded at 25 °C on a Cary 3 spectrophotometer. Absorbances at 290 and 278 nm were obtained from zero-order spectra acquired from 250 to 310 nm. Second-derivative spectra were derived from the zero-order spectra using an in-house computer program based on the method by Savitsky and Golay (*23*). The concentrations of pGH used were 0.22 and 2.0 mg/mL.

Size-Exclusion Chromatography. Hydrodynamic radii were determined using a Superose 12 HR10/30 column (30 × 1.0 cm i.d.) with a Pharmacia FPLC system. A stock solution of pGH (10 mg/mL) in 5 mM sodium bicarbonate, pH 8.0, was diluted to a final concentration of 0.22 mg/mL in 100 mM sodium phosphate/4 M urea at pH 8.0 and pH 2.0. A 100 μL sample was injected onto a Superose 12 column preequilibrated in 100 mM sodium phosphate at the same pH and urea concentration as the sample. The flow rate used was 0.5 mL/min. Protein elution was monitored by the absorbance at 280 nm. Protein molecular weight calibration curves for the Superose 12 column in 6 M Gdn-HCl were determined and utilized to calculate the Stokes radius of pGH at each pH (*24*).

Circular Dichroism. CD spectra were recorded using a Jasco J-720 spectropolarimeter. Stock solutions of pGH (8.8 and 2.2 g/L) in 5 mM sodium bicarbonate, pH 7.5, were diluted 10-fold with either 25 mM Na_2HPO_4/25 mM sodium acetate ± 4 M urea or 100 mM Na_2HPO_4/25 mM sodium acetate ± 4 M urea, which had been adjusted to various pH values. The final protein concentrations (∼0.88 and ∼0.22 g/L) were determined by reading the absorbance at 278 nm (corrected for light scattering at 350 nm) and using an extinction coefficient of 15 714 M^{-1} cm^{-1} (*21*). The absorbance at 350 nm was always ≤5% of the absorbance at 278 nm. The pH of each diluted protein sample was checked using a narrow-bore pH probe (Amicon).

Samples were kept at 25 °C in the spectropolarimeter using a water-jacketed cell holder connected to a Neslab RT-111 water bath. For far-UV spectra (180−260 nm), four to six scans of 0.22 g/L protein in 0.1 cm path-length cells were coadded. For near-UV spectra (260−310 nm), six to ten scans of 0.88 g/L protein in 1 cm path-length cells were coadded. The spectra of buffer collected in the same manner were subtracted from the sample spectra. Data were converted to mean residue ellipticity, $[\theta]_{MRW}$, using a mean residue weight of 114.5.

Sedimentation Equilibrium Using Analytical Ultracentrifugation. Sedimentation equilibrium experiments were performed using a Beckman XL-A analytical ultracentrifuge set at 25 °C. The ultracentrifuge cells were fitted with Yphantis-style six-channel centerpieces. Three different concentrations (typically 2, 1, and 0.5 g/L) of sample (125 μL) were loaded parallel to the solvent channels containing buffer alone (130 μL). The final concentrations of buffer components were 80 mM Na_2HPO_4/20 mM sodium acetate/1 mM sodium bicarbonate ± 4 M urea, pH 8 or pH 2.

Samples were centrifuged to sedimentation equilibrium at speeds of 9000−27 000 rpm. Scans were collected in continuous scan mode (0.01 cm steps, 13 acquisitions per step) at 2−4 h intervals using wavelengths of 280−300 and 350 nm. Sedimentation equilibrium was judged to have been reached when the difference in concentration distribution between two consecutive scans was zero. Baseline deviations were corrected by subtracting the scans collected at 350 nm from those collected at 280−300 nm.

Sedimentation Equilibrium Data Treatment and Model Fitting.[2] Apparent point-average weight-average molecular weight values ($M_{w,app}$) were calculated from plots of $\ln[c(r)]$

[2] A package of programs for the workup of raw data and for the fitting of models is available via anonymous FTP at the address bbri.harvard.org. Change to directory rasmb.spin.ms_dos.sedprog-ralston.

versus r_2 plots (*25*), where $c(r)$ is the concentration of protein (g/L) at radial position r.

Plots of $M_{w,app}$ versus concentration are qualitatively useful in assessing the self-association of a solute (Figure 6), but substantial error is introduced into $M_{w,app}$ values through a numerical differentiation step. Therefore, as a means of assessing the quality of the sedimentation equilibrium data and for the purposes of fitting self-association models, we replotted the data in terms of the Ω function, $\Omega(r)$ (*26*).

$$\Omega(r) = \frac{c(r)\exp[\phi_1 M_1(r_F^2 - r^2)]}{c(r_F)} \quad (1a)$$

$$= \frac{a_1(r_F)c(r)}{a_1(r)c(r_F)} \quad (1b)$$

where $\phi = (1 - \bar{v}\rho)\omega^2/2RT$, $\bar{v}$ is the partial specific volume of the protomer in milliliters per gram, ρ is the density of the solvent in grams per milliliter, and ω is the angular velocity in radians per second. M_1 is the molar mass of the protomer (the smallest species participating in the self-association of the protein), $c(r_F)$ is the total concentration of protein at the radial reference position r_F, and a_1 is the thermodynamic activity of the protomer. A value of 0.737 mL/g was used for $\bar{v}$ calculated from the sequence (*15*) using the method of Cohn and Edsall (*27*). The value of ρ was calculated from the density of the buffer components and water using the program SEDNTERP v1.03 (Amgen). In some cases, the value of M_1 used was that of the pGH monomer (21 860), while in others, no detectable monomer was present and the value of M_1 used was that of the dimer (43 720).

Plots of $\Omega(r)$ versus $c(r)$ for the three loading concentrations of protein at sedimentation equilibrium were calculated using a common value of $c(r_F)$ (e.g., Figure 7A). Overlap of the data over the common concentration range is a very sensitive indicator that both chemical and sedimentation equilibria have been attained (*26*, *28*); i.e., overlap indicates that pGH was pure and that all pGH molecules were able to participate in the self-association and no irreversible aggregates were formed.

The Ω data were fitted with models of discrete (e.g., monomer−dimer) and indefinite (e.g., SEK 1; *29*) self-association (e.g., Figure 7B). For each model, the concentration of the protomer, $c_1(r)$, was written as an explicit or implicit function of $c(r)$. The SEK 1 model describes the sequential addition of protomers, P, where the addition of each protomer is described by a single molar equilibrium constant, K:

$$P \overset{K}{\rightleftharpoons} P_2 \overset{K}{\rightleftharpoons} P_3 \overset{K}{\rightleftharpoons} P_4 \ldots \overset{K}{\rightleftharpoons} \ldots P_n$$

$$c(r) = c_1(r)/[1 - kc_1(r)]^2 \qquad \text{if } kc_1(r) < 1 \quad (2)$$

where $k = K/M_1$.

For all models, the Adams−Fujita approximation (*30*) was used to relate the thermodynamic activity of the protomer, $a_1(r)$, to the concentration of protomer, $c_1(r)$:

$$a_1(r) = c_1(r)\exp[BM_1c(r)] \quad (3)$$

where B, the second virial coefficient, is a measure of the nonideality of the solute which principally arises from the size and shape of the solute and its effective charge in the buffer conditions employed. With this approximation, a single value of B is sufficient to describe all species in a self-association so that, for example, the nonideality of the solute monomer would equal B, that of the dimer would equal $2B$, etc.

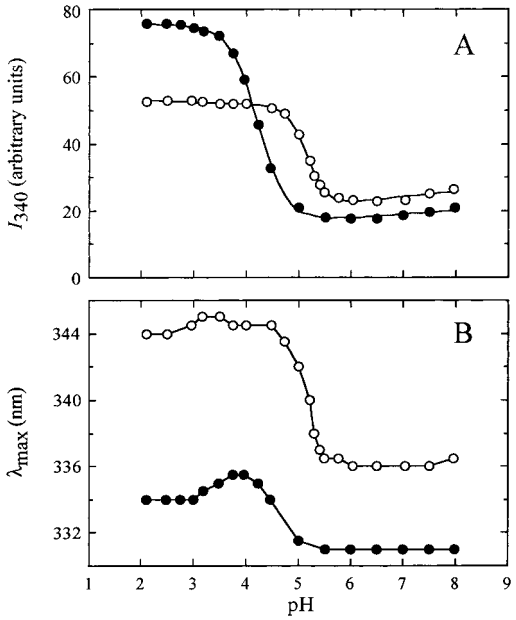

FIGURE 1: (A) Acid-induced denaturation of pGH as measured by intrinsic tryptophan fluorescence at 340 nm (I_{340}). The protein concentration was 0.22 mg/mL in buffer containing 20 mM each of sodium acetate, sodium bicarbonate, MES, and Tris-HCl ± 4 M urea at various pH values. Excitation was at 295 nm. (B) Effect of pH on the fluorescence emission maximum (λ_{max}) of pGH. Symbols represent (●) −4 M urea and (○) +4 M urea.

The models were fitted to the Ω function data by nonlinear regression (*28*, *31*). Values of the thermodynamic parameters, K and B, ±SE, were returned where SE is the approximate (asymptotic) standard error of the variable parameter calculated from the inverse matrix set up from partial derivative equations of the fitting function (*32*). Models which appropriately described the data resulted in a random distribution of residuals (e.g., Figure 7C) as determined by a runs test at the 5% level.

RESULTS

Conformational Changes Determined by Fluorescence Spectroscopy. The fluorescence emission of tryptophan is highly sensitive to the polarity of its environment, thus providing a useful tool for probing conformational changes in proteins. We have measured the fluorescence emission of the single tryptophan of pGH, located at residue 86 in helix 2, to follow the conformational changes upon acidification of pGH in both the presence and absence of 4 M urea. In the absence of urea, the relative fluorescence intensity at 340 nm (I_{340}) of 0.22 mg/mL pGH (10 μM) exhibited a 4-fold increase through the transition from pH 8 to pH 2 (Figure 1A). The apparent midpoint of the transition was at pH 4.10 (Figure 1A). A small red shift, from 331 ± 1.0 nm at pH 8 to 334 ± 1.0 nm at pH 2.0, in the wavelength of maximum emission (λ_{max}) was observed (Figure 1B).

In the presence of 4 M urea, the I_{340} of 0.22 mg/mL pGH increased 2.5-fold across the transition from pH 8 to pH 2

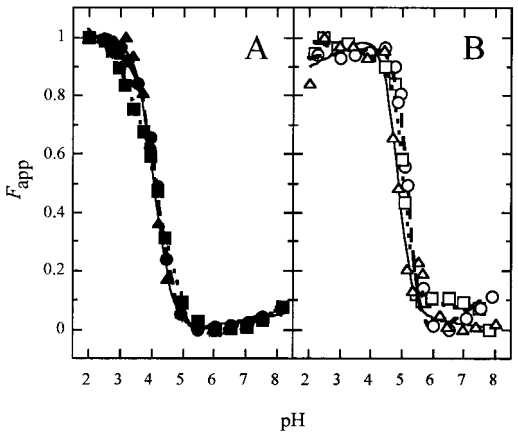

FIGURE 2: Effect of protein concentration on the acid-induced denaturation of pGH as measured by intrinsic tryptophan fluorescence at 340 nm. Data are expressed as the apparent fraction of unfolded pGH as a function of pH: $F_{app} = (I_{obs} - I_{nat})/(I_{unf} - I_{nat})$, where I_{obs} is the observed fluorescence intensity at 340 nm and I_{nat} and I_{unf} are the observed values for the native and unfolded forms, respectively. (A) Effect of protein concentration in the absence of 4 M urea: 0.05 mg/mL (■); 0.22 mg/mL (●); 0.5 mg/mL (▲). (B) Effect of protein concentration in the presence of 4 M urea: 0.05 mg/mL (□); 0.22 mg/mL (○); 0.5 mg/mL (△). Data are fitted using the method of Pace (*33*): 0.05 g/L (···); 0.22 g/L (---); 0.5 g/L (—).

(Figure 1A). The apparent midpoint of the transition was at pH 5.16 (Figure 1A). The λ_{max} increased from 336 ± 1.0 nm at pH 8.0 to 344 ± 1.0 nm at pH 2.0 (Figure 1B).

The effect of protein concentration on the acid-induced denaturation was examined at 0.05, 0.22, and 0.5 mg/mL pGH in the presence and absence of 4 M urea (Figure 2). Assuming a two-state mechanism, the transitions observed at each protein concentration were compared by plotting the apparent fraction of the unfolded protein, F_{app}, versus pH

$$F_{app} = (I_{obs} - I_{nat})/(I_{unf} - I_{nat})$$

where I_{obs} is the observed I_{340} at a given pH and I_{nat} and I_{unf} are the observed values for the native and unfolded forms, respectively, extrapolated to each point in the transition zone (*33*). Least-squares analysis of the experimental data was used to determine I_{nat} and I_{unf} in the pre- and post-transition zone (*33*). Transitions in the absence of urea are almost superimposable with midpoints centered at pH 4.1 (Table 1). In the presence of 4 M urea, the transition midpoints are centered at pH ~5.2 (Table 1), and the transitions are sharper.

Conformational Changes Followed by UV Absorbance. The zero-order UV absorbance spectra of native pGH at pH 8 ± 4 M urea display an absorption maximum at 278 ± 0.1 nm. The prominent shoulder centered near 290 nm is due mainly to the absorption of the single tryptophan residue (Figure 3A). Acidification from pH 8 to pH 2 in the absence of 4 M urea produced a general blue shift in the spectrum with the absorption maximum shifted to 276.5 ± 0.2 nm (Figure 3A). In the presence of 4 M urea, a similar blue shift in the absorption maximum to 276.2 ± 0.2 nm is observed at pH 2.0. In addition, there is a red shift in the spectrum at wavelengths above ~293 nm (Figure 3A).

A plot of the molar extinction coefficient at 290 nm (ϵ_{290}) as a function of pH reveals a decrease (hypochromicity) of ~2500 and ~2100 M^{-1} cm^{-1}, with midpoints at pH 5.11 and pH 3.59, in the presence and absence of 4 M urea, respectively (Figure 3C). As observed in the fluorescence studies, the inclusion of 4 M urea yields a sharper transition upon acidification.

In zero-order absorption spectra, contributions from both tyrosine and tryptophan residues overlap considerably.

Table 1: Midpoints of the Acid-Induced Transitions of pGH, in the Presence and Absence of Urea, Measured by Different Spectroscopic Techniques

measurement	protein concn (g/L)	midpoint[a]		no. of expts
		−4 M urea	+4 M urea	
I_{340}	0.05	4.10 ± 0.02	4.93 ± 0.04	2
I_{340}	0.22	4.08 ± 0.06	5.16 ± 0.06	3
I_{340}	0.50	4.10 ± 0.05	5.02 ± 0.03	2
ϵ_{290}	0.22	3.59 ± 0.03	5.11 ± 0.04	3
θ_{285}	0.22	3.94 ± 0.03	5.42 ± 0.08	1
θ_{300}	0.22	nt	5.24 ± 0.03	1
θ_{222}	0.22	3.89 ± 0.04	5.18 ± 0.05	1

[a] Data fitted by nonlinear regression using the equation described by Pace (*33*) for I_{340} or using a sigmoidal function (*22*). Errors represent the standard error (*32*) returned from the nonlinear regression fit (n = 1), the range of values (n = 2), or the standard error of the mean value (n = 3). nt = no transition.

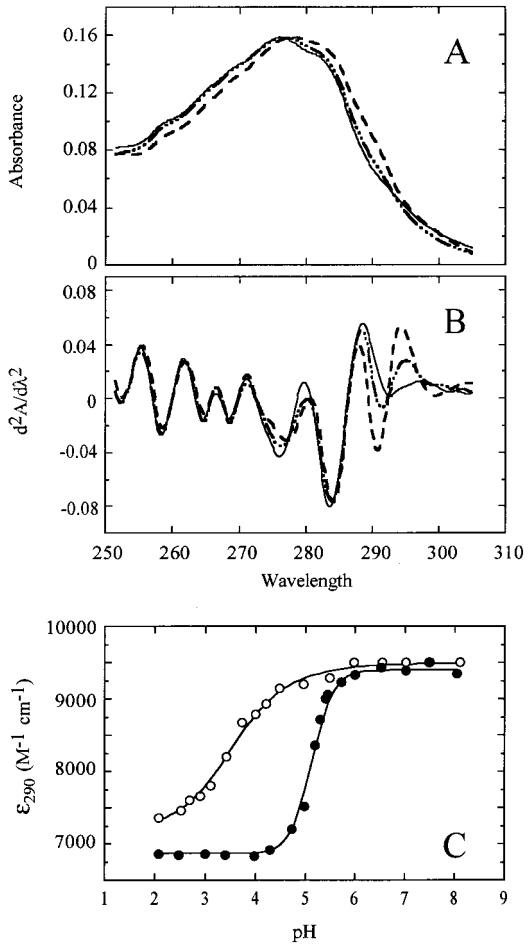

FIGURE 3: Acid-induced denaturation of pGH as monitored by UV absorbance. The protein concentration was 0.22 mg/mL in buffer containing 20 mM each of sodium acetate, sodium bicarbonate, MES, and Tris-HCl ± 4 M urea. (A) Zero-order absorbance spectra at pH 8 ± 4 M urea (---), pH 2 (-···-), and pH 2 + 4 M urea (—). (B) Second-order derivative spectra ($d^2A/d\lambda^2$) obtained from the zero-order absorbance spectra at pH 8 ± 4 M urea (---), pH 2.0 (-···-), and pH 2.0 + 4 M urea (—). (C) Effect of pH on the absorbance at 290 nm (ϵ_{290}) in the absence (●) and presence (○) of 4 M urea.

Resolution can be improved and peak positions more accurately located if the derivative of absorbance with respect to wavelength is calculated (*34*). Figure 3B shows the calculated second derivative of each of the zero-order absorption spectra shown in Figure 3A. Note the correspondence of the minima in the second derivative of the absorption spectrum with the peaks and shoulders in the zero-order absorption spectrum.

The wavelength minima attributed to the phenylalanine chromophores in the 250−270 nm region of the spectrum (*35*) do not change in the four conditions examined, indicating no net change in the average polarity of these chromophores.

The blue shift seen in the zero-order absorption maximum (Figure 3A) can be more clearly seen as a minimum in the 276−278 nm region (Figure 3B); this band is attributed to one of the higher vibrational modes of the Tyr ^1L_b transition. There is no significant change in the wavelength of the 284 nm minimum, attributed to the Tyr ^1L_b [0-0] transition (*35*).

The red shift above 293 nm seen in the zero-order spectrum at pH 2.0 in the presence of 4 M urea (Figure 3A) is due to a red shift in the Trp ^1L_b band from 290.9 nm at pH 8 (±4 M urea) to 291.5 (pH 2) and 292.6 nm (pH 2 + 4 M urea) (Figure 3B). At pH 8, the inclusion of 4 M urea results in a decrease in the intensity of the Trp ^1L_a [0-0] band at 299.5 nm. In studies using hGH, Bewley and Li (*35*) predicted that the extent of the red shift of this band compared to its [0-0] position in water of 292 nm correlates with the strength and alignment of a hydrogen bond between the indole ring >NH of Trp86 and a carboxylate residue. However, for pGH at pH 2 ± 4 M urea, the Trp ^1L_a signal is difficult to identify possibly due to blue shifting into the intense positive band centered near 295 nm (Figure 3B).

Conformational Changes Determined by Circular Dichroism. A decrease in the CD intensity in the near-UV is usually associated with a loss of tertiary structure or a localized unfolding of the protein in the vicinity of a particular aromatic group. Figure 4A shows the near-UV CD spectra for pGH at pH 8 and pH 2 in the absence and presence of 4 M urea. At pH 2 in the absence of urea, most of the tyrosine-attributed signal at 285 nm is lost. A plot of mean residue ellipticity ($[\theta]_{MRW}$) at 285 nm, θ_{285}, versus pH showed midpoints centered at pH 3.94 and pH 5.42 in the absence and presence of 4 M urea, respectively (Figure 4B).

Figure 4A also shows that there is a weak broad band centered at 298 nm which at pH 2 + 4 M urea becomes the prominent band in the spectrum. Figure 4C shows the effect of pH on the $[\theta]_{MRW}$ at 300 nm, θ_{300}, in the presence and absence of 4 M urea. In the presence of 4 M urea, the midpoint of the transition is centered at pH 5.24. The increase in θ_{300} observed here is comparable to that seen in the Gdn-HCl-induced self-association of bGH (*36*) and pGH (*21*, *37*).

Far-UV CD was used to monitor changes in secondary structure by measurement of $[\theta]_{MRW}$ at 222 nm, θ_{222} (Figure 4D). A decrease in θ_{222} of approximately 15% and 25% in the absence and presence of 4 M urea, respectively, was observed.

Size-Exclusion Chromatography. Previous studies have used size-exclusion chromatography to determine the hydrodynamic radii of the multiple forms present during the Gdn-HCl-induced unfolding of pGH and bGH (*21*, *38*).

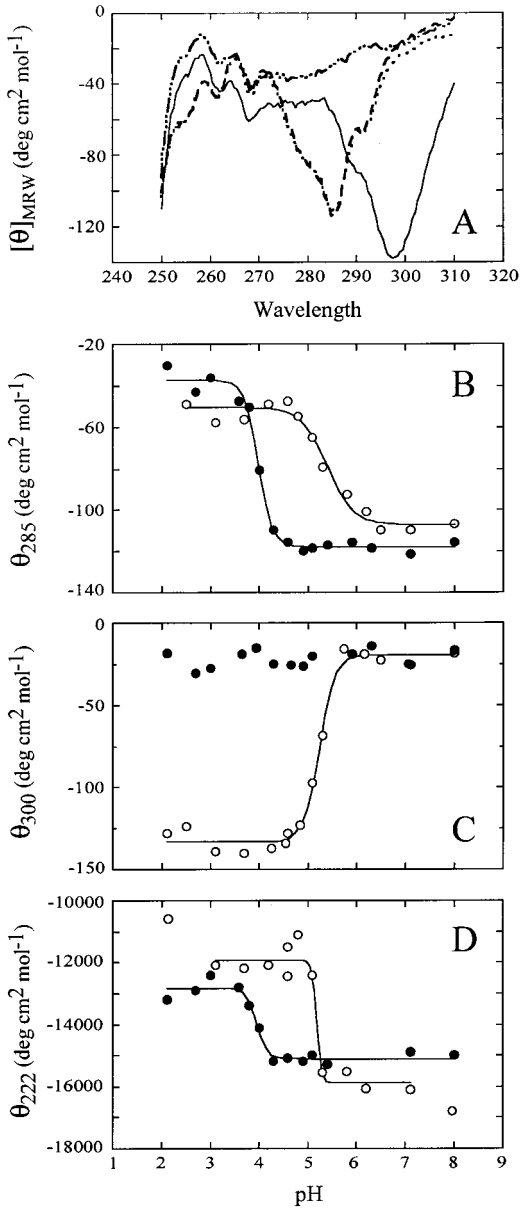

FIGURE 4: Acid-induced denaturation of pGH as monitored by far- and near-UV CD. The protein concentration was 0.22 mg/mL in 80 mM sodium phosphate/20 mM sodium acetate ± 4 M urea. (A) Near-UV spectra of pGH at pH 8 (---), pH 8 + 4 M urea (···), pH 2.0 (-···-), and pH 2.0 + 4 M urea (—). Effect of pH on the mean residue ellipticity at (B) 285 nm, (C) 300 nm, and (D) 222 nm, in the absence (●) and presence (○) of 4 M urea.

Figure 5 shows the elution profiles of pGH in the presence of 4 M urea, at pH 8 and pH 2. In the absence of urea, no protein was recovered from the column between pH 5 and pH 2, presumably due to nonspecific interaction with the column matrix. Even in the presence of 4 M urea, recovery in this pH region was greatly reduced. At pH 8, a single peak with a radius of 18 Å, consistent with pGH in the folded state (*21*), was observed (Figure 5). At pH 2, the majority of the protein eluted earlier, with a hydrodynamic radius of 47 Å. The elution volume of this peak was very close to that previously seen for the Gdn-HCl-induced associated form of pGH (*21*). The second, smaller peak at pH 2, with a radius comparable to that of the folded state of pGH at pH 8, is consistent with that of the monomer partially denatured by acid.

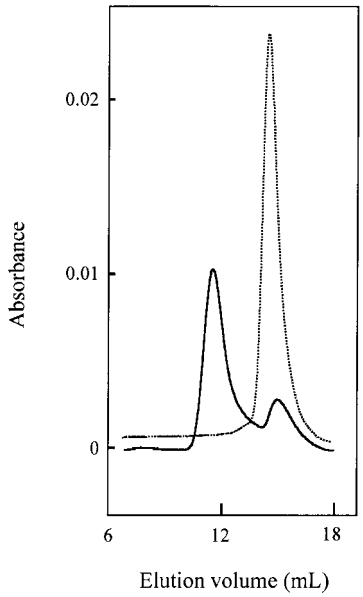

FIGURE 5: Size-exclusion chromatograms for pGH eluted from a Superose 12 column at pH 8.0 + 4 M urea (···) and pH 2.0 + 4 M urea (—). The protein concentration upon injection was 0.22 mg/mL, and elution of protein was monitored by absorbance at 280 nm.

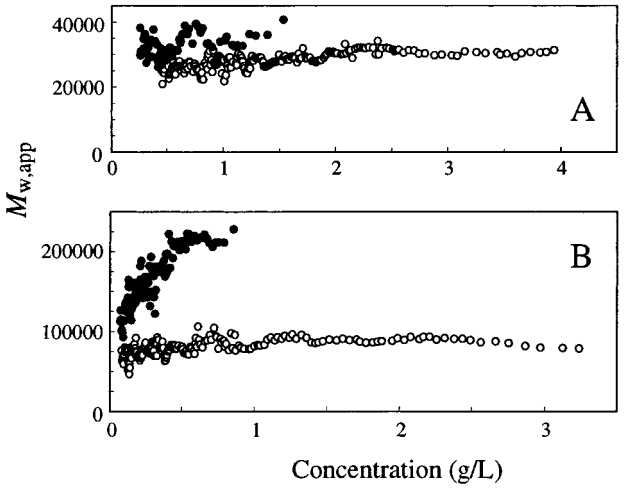

FIGURE 6: Self-association of pGH as measured by sedimentation equilibrium in the analytical ultracentrifuge. Apparent weight-average molecular weight values ($M_{w,app}$) were calculated from absorbance values measured from the equilibrium distribution of protein in the ultracentrifuge cell. Data obtained at pH 8 (A) and pH 2 (B) in the absence (●) and presence (○) of 4 M urea. Each data point represents an average of three values taken from three separate concentration gradients centrifuged to equilibrium (see Experimental Procedures for details).

Self-Association of pGH Measured by Sedimentation Equilibrium. We have also examined the ability of pGH to self-associate using the thermodynamically rigorous technique of sedimentation equilibrium in the analytical ultracentrifuge. Figure 6 shows the apparent weight-average molecular weight ($M_{w,app}$) distributions for pGH at sedimentation equilibrium at pH values of 8 and 2 ± 4 M urea. Self-association takes place under all conditions and is strongly promoted by the drop in pH and by the absence of urea at either pH.

Figure 7A shows a typical plot of the Ω function versus radial concentration of pGH at sedimentation equilibrium for three different loading concentrations of pGH. The overlap

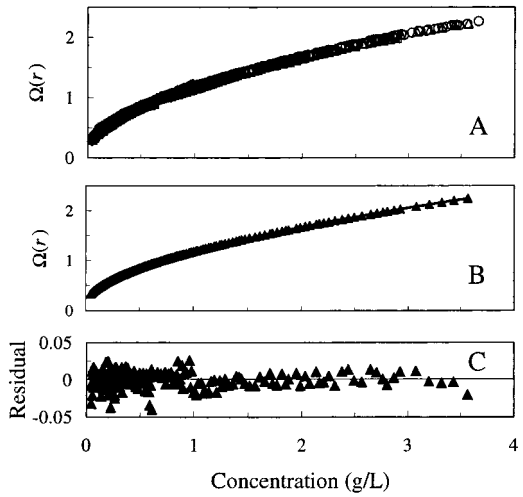

FIGURE 7: Analysis of sedimentation equilibrium data of pGH using the Ω function. (A) In this example, four different loading concentrations of pGH (◇, 0.5 g/L; ○, 1 g/L; △, 1.5 g/L; □, 2 g/L) at pH 2 + 4 M urea were centrifuged at 15 000 rpm to equilibrium. The absorbance values measured from the equilibrium distribution of protein were converted to Ω values using a reference concentration [$c(r_F)$] of 0.7 g/L and a molecular weight of the protomer of 43 720 (equivalent to the dimer of pGH). The overlap of the data from the separate loading concentrations indicates that all steps in the self-association of pGH are fully reversible and that the sample is homogeneous. In (B), the data from (A) were averaged four points at a time and fitted (solid line) with a self-association model describing dimers of pGH associating to form tetramers and octamers. The returned values of the parameters are shown in Table 2. (C) Residuals of the fit shown in (B). A runs test showed that the distribution of the residuals was random.

of the data shows that all pGH molecules were able to participate in the self-association and no irreversible aggregates were formed (see Experimental Procedures for details). Self-association models were fitted to the Ω plots and returned estimates of the thermodynamic parameters, the molar equilibrium constant(s), *K*, and the second virial coefficient, *B*, a measure of the nonideality of the solute. (Figure 7B; Table 2; see Experimental Procedures). Models which appropriately described the data resulted in a random distribution of residuals (e.g., Figure 7C) as determined by a runs test at the 5% level.

At pH 8 + 4 M urea, a monomer−dimer model adequately describes the data over an extended concentration range (0.4−4 g/L), and the self-association, as judged by the value of *K*, is very weak (Table 2). The returned value of *B* was $(4.3 \pm 0.6) \times 10^{-7}$ L mol g^{-2}. On the basis of the estimated charge of pGH[3] and a Stokes radius of 2.2 nm (*40*), we calculate a theoretical value of 4.5×10^{-7} L mol g^{-2} (*31*, *41*).

In the absence of urea at pH 8, a monomer−dimer model fit the Ω plot well but returned a negative (and therefore physically meaningless) value of *B* (data not shown). A negative value of *B* indicates that the self-association model underestimates the number and/or size of the oligomers that are present at significant concentration. On the other hand, the "indefinite" SEK 1 model, in which a single value of *K* describes the sequential addition of monomers without limit

[3] A charge of −2 was estimated for pGH on the basis of its amino acid sequence and using standard pK_a values for the residues. Counterion binding is expected to reduce the net charge by ∼50% (*39*).

Table 2: Sedimentation Equilibrium Results for pGH under Various Solution Conditions[a]

	model	K (M^{-1}) $\times 10^{-5}$	B (L mol g^{-2}) $\times 10^{-7}$
pH 8	monomer−dimer−tetramer[b]	0.29 ± 0.03 (K_{12}) 0.025 ± 0.06 (K_{24})	4.5[d]
pH 8 + 4 M urea	monomer−dimer	0.056 ± 0.001	4.3 ± 0.6
pH 2	SEK 1 (dimer, tetramer, hexamer, etc.)	7.5 ± 0.2	22.3 ± 1.6
pH 2 + 4 M urea	dimer−tetramer−octamer[c]	7.3 ± 0.6 (K_{24}) 0.085 ± 0.09 (K_{48})	6.2 ± 1.1

[a] Plots of $\Omega(r)$ versus $c(r)$ were fitted with self-association models using nonlinear regression techniques. Returned values of the equilibrium constants, K, and the second virial coefficient, B, are shown ± standard error. [b] A monomer−dimer−trimer model fit the data equally well on the basis of sums of squares of the residuals and random distribution of residuals as judged by the runs test. [c] A dimer−tetramer−hexamer model fit the data equally well on the basis of sums of squares of the residuals and random distribution of residuals as judged by the runs test. [d] Parameter value fixed during nonlinear regression. A theoretical value for B, B_T, was calculated from the size and shape of the solute (B_E) plus a contribution from the net charge on the solute (B_C) (*31*, *41*; see text for further details).

(see Experimental Procedures for details) returned a value of B an order of magnitude larger than the theoretical value. When the value of B was fixed at the theoretical value, both the monomer−dimer−trimer and monomer−dimer−tetramer fit the data equally well with the value of K for the monomer−dimer step ~5 times larger than that obtained in the presence of urea (Table 2). Thus, in the absence of urea both the strength and extent of self-association of pGH are increased. Other types of discrete self-association (e.g., monomer−trimer or monomer−tetramer) resulted in poor fits to the data as judged by the sums of squares of the residuals and a runs test performed on the distribution of the residuals.

At pH 2, self-association was strongly promoted (Figure 6B) to the extent that significant concentrations of monomeric pGH could not be detected over the total concentration ranges observed. Note that the values of $M_{w,app}$ at very low concentration at pH 2 ± urea are larger than the monomer molecular weight of 21 860, indicating that the protomer for self-association was larger than the monomer. To confirm this, plots of the Ω function versus concentration were generated using the molecular weight of the monomer and small values (~0.2 g/L) of the reference concentration, $c(r_F)$. Fits to these plots with various self-association models, using the monomer as the protomer, passed through or very close to the origin (data not shown). This shows that no detectable monomer was present at the reference concentration and that the protomer for the self-association was the dimer or some larger species (*26*, *28*, *31*). Therefore, we used self-association models at pH 2 in which the protomer was taken to be the dimer.

At pH 2 in the absence of urea, the SEK 1 model (dimer, tetramer, hexamer, ...) fit the data well, and the returned value of K describing the sequential steps in the self-association was 1−3 orders of magnitude larger than values of K obtained at pH 8 ± urea (Table 2). [Extrapolation of the fit for this model to zero concentration confirmed that a significant percentage (9%) of the protein at the reference concentration of 0.5 g/L was in the form of the dimer.]

At pH 2 + 4 M urea, two discrete models, dimer−tetramer−hexamer and dimer−tetramer−octamer, fit the data equally well. As at pH 8, the presence of 4 M urea reduced both the strength and extent of self-association (Table 2).

DISCUSSION

In protein folding studies, the presence and concentration of intermediates are dependent upon a number of factors. These include pH, temperature, the concentrations of salts and denaturants, and, importantly, the intrinsic properties of the protein employed (*3*, *13*). For acid-mediated partial unfolding, three broad classes of protein have been recognized: (I) those that unfold and then refold to a molten globule, (II) those that unfold via the molten globule, and (III) those that remain essentially native (*13*). hGH falls into category III, while bGH falls into category II. This study shows that acid-induced unfolding of pGH also falls into category II with folding intermediates that possess many of the classic characteristics of the molten globule. These characteristics include retention of substantial secondary structure, substantial loss of tertiary structure, maintenance of a compact shape similar in size to that of the native state, and a propensity to aggregate. However, the folding intermediates for pGH and bGH have quite distinct properties, emphasizing the range of structural variability of intermediates even among closely related proteins.

pH-Dependent Unfolding of pGH in the Absence of Urea. A comparison of the unfolding transition midpoints is shown in Table 1. In the absence of urea, the midpoints of the transitions obtained for the three probes of tertiary structure (I_{340}, θ_{285}, and ϵ_{290}) are not coincident. The lack of coincidence indicates that conformational changes affecting the intrinsic fluorescence, I_{340}, of Trp86 (Figure 1) occur prior to conformational changes affecting the arrangement of other chromophores (Figures 3 and 4).

For Trp86, the 4-fold increase in I_{340} (Figure 1A) is accompanied by a 3 nm red shift in the λ_{max} with decreasing pH (Figure 1B). This compares with a red shift of 14 nm for the complete unfolding of pGH at near neutral pH by 6 M Gdn-HCl (*21*). The increase in the relative fluorescence intensity with minimal change in the λ_{max} suggests removal of an intramolecular quenching group without a significant change in the polarity of the environment surrounding Trp86.

Elucidation of the residue(s) responsible for the quenching of the native state tryptophan fluorescence of bGH and pGH has proved elusive (*18*), but the pH midpoint for I_{340} suggests that the removal of the quenching group is mediated by the titration of Glu and/or Asp residues. A model of pGH (*42*) based on the hGH/hGH receptor crystal structure (*16*) shows that Trp86 is located in a hydrophobic core composed of Phe54, Ser55, Leu82, Ile83, Ser85, Leu87, Pro89, Val90, Leu93, Leu113, Leu161, Cys164, Phe165, and Asp168. The obvious quenching group is Asp168, which, as seen in hGH (*16*), is hydrogen bonded to the Nϵ1 of Trp86. However, all of the above residues, including Asp168, are conserved in hGH, which, unlike pGH and bGH, does not have a quenched native state fluorescence (*18*, *43*). The Cys53−Cys164 disulfide bridge may be the Trp fluorescence quencher in native pGH and bGH (*18*) since subtle structural differences between the native conformations of growth hormones could

result in different orientations of the disulfide bridge with respect to Trp86.

The reduction in molar absorption at 290 nm (ϵ_{290}) by 2000 M^{-1} cm^{-1} with decreasing pH (Figure 3C) is similar to that previously seen in the Gdn-HCl-induced denaturation of pGH and bGH (*21*, *42*). In those studies, the decrease in ϵ_{290} was attributed to the removal of the internalized Trp86 to the polar solvent exterior. In this case, the lack of red shift in the λ_{max} of fluorescence emission coupled with the loss of the near-UV CD signal at 285 nm (θ_{285}; Figure 4B) suggests that a change in the average environment of the seven tyrosine residues of pGH is responsible for a significant proportion of the ϵ_{290} loss. A similar conclusion was made in the early acid-induced denaturation studies of bGH (*44*). The reduction in absorbance at 290 nm produced by transfer of a Tyr residue from the protein interior to water is ~600 M^{-1} cm^{-1} (*45*). A model of pGH (*42*) shows that Tyr159 is completely buried while Tyr29 and Tyr175 are almost fully buried. Exposure of these residues to solvent is indicated by the loss of the θ_{285} signal with decreasing pH (Figure 4A) and would be responsible for a significant proportion of the observed hypochromicity.

pH-Dependent Unfolding of pGH in the Presence of 4 M Urea. The inclusion of 4 M urea in the acid-induced unfolding results in a pGH population with similar loss of the asymmetrical environment of tyrosines (Figure 4B), similar loss of α-helix (Figure 4D), and similar hypochromicity (Figure 3C) as that observed in the absence of urea.

There are also clear differences in the intermediates observed at pH 2 in the presence and absence of urea and in the pH-dependent transitions that lead to those intermediates. At pH 2 + urea, λ_{max} for intrinsic fluorescence red shifts by 8 nm (Figure 1B), indicating increased, but not necessarily complete, exposure of Trp86 to the solvent. An intense CD band is observed near 300 nm at pH 2 + urea (Figure 4A), indicating that Trp86 is in a highly asymmetric environment despite its increased solvent exposure. A similar band has been observed for bGH in 4 M Gdn-HCl, pH 8.5 (*36*), indicating some similarity between the intermediates formed by these two growth hormones under different solvent conditions.

The acid-induced unfolding transitions observed in the presence of urea are shifted up by ~1 pH unit compared to those in the absence of urea (Table 1). The shift to higher pH is unlikely to result from a shift in pK_a of titrated carboxylic acid groups. The inclusion of chemical denaturants during acid titration of proteins generally normalizes the pK_a values of titratable groups to those found for the free amino acids in solution. For Asp and Glu residues, these values are ~3.9 and 4.3, respectively, well below the apparent pH midpoint of ~5.2. In their study on bGH, Edelhoch and Burger (*46*) also observed a shift in the midpoint of the acid transition to higher pH values in the presence of increasing urea concentrations. They claimed that the shift in the midpoints to higher pH could not be attributed to a shift in the pK_a of carboxyl groups.

It is more likely that the shift in the pH midpoint in the presence of 4 M urea results from the titration of one or more critical histidines. A change in the pK_a for a histidyl side chain from a value below that of the transition pH in the native state to a value higher than the transition pH in the intermediate would promote a shift in the chemical equilibrium toward the intermediate (*47*), as dictated by Le Chatelier's principle.

In the model of the structure of pGH, histidines 22 and 170 are within hydrogen-bonding distance of each other (<3 Å), located in a shallow cleft which roughly divides the molecule in two (*42*). Their interaction may produce a situation qualitatively similar to that seen for His24 and His119 in apomyoglobin (*47*). In native apomyoglobin, His24 is hydrogen bonded to His119, resulting in a very low pK_a for His24 of ~3. His24 is not protonated until the native state unfolds to the intermediate whereupon its pK_a is raised to ~6.5 (*47*). This change in pK_a largely dictates the acid-induced unfolding of apomyoglobin to its intermediate with a transition midpoint at pH 4.4 (*47*). In bGH, early NMR studies showed that either His20 or His22, located on helix 1, has a low value of pK_a (4.67; *48*). Due to the combined effects of its partially buried location (*42*) and its interaction with His170, we speculate that it is His22 in pGH that has the depressed value of pK_a in the native state. In the acid plus urea-induced intermediate, the pK_a of His22 would need to be raised above the transition midpoint of ~5.2 to serve as a driving force for the formation of the intermediate. In hGH, due to the insertion of an amino acid in the primary sequence separating the helix 1 histidines, both are located on the solvent-exposed face of the helix (*16*). Furthermore, the equivalent position for His170 in pGH is occupied by aspartate in hGH.

Self-Association of Native pGH and pGH Unfolding Intermediates. Using size-exclusion chromatography, we were unable to elute protein in the absence of urea possibly because the protein irreversibly adhered to the matrix. In 4 M urea at pH 2 (Figure 5), 69% of the protein was recovered in two peaks, the early eluting peak corresponding to an associated form (*21*). Sedimentation equilibrium was used to quantify the mode, strength, and reversibility of the self-association of pGH under various solution conditions. Our data show that pGH self-associates reversibly at pH 8 (Figure 6, Table 2) whereas native hGH does not self-associate (*49*). Results from less rigorous methods indicate that native bGH is monomeric (*36*), but no sedimentation equilibrium data are available, as far as we are aware.

The sedimentation equilibrium results for pGH (Figures 6 and 7) highlight the problem of relying solely on nonthermodynamic methods such as size-exclusion chromatography and correlations with other physical phenomena to quantify the self-association of proteins in general and growth hormones in particular. For example, the use of size-exclusion chromatography, tryptophan fluorescence, and circular dichroism has not resulted in a satisfactory determination of the mode and strength of the self-association of bGH folding intermediates (*36*, *50*). Brems, Havel, and coworkers frequently used changes in the value of θ_{300} as a measure of the self-association of folding intermediates of bGH (*36*, *50*). However, it is clear from our results with pGH that not all intermediates result in the generation of a θ_{300} signal (Figure 4A,C), and, in fact, the strongest self-association we observe (pH 2 minus urea) is not accompanied by changes in θ_{300} (Figure 6, Table 2). Thus, the use of θ_{300} as a measure of self-association may partly or completely underestimate the level of self-association.

Figure 8 shows models of the self-association of pGH under the four conditions used in this study. Both urea and

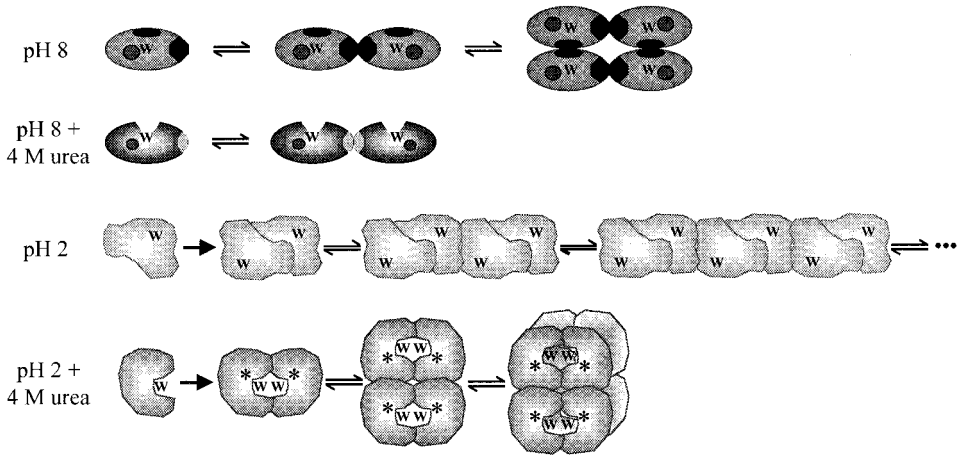

FIGURE 8: Theoretical models of the modes of self-association of pGH under various solvent conditions. The solid arrows, describing the first step at pH 2 and at pH 2 + 4 M urea, represent equilibria which could not be observed over the concentration range of pGH measured in the sedimentation equilibrium experiments. The association constants are estimated to be $\geq 5 \times 10^6$ M^{-1}. All other steps are represented by equilibrium signs, and the values of the constants for these fully reversible self-association steps are shown in Table 2. W represents Trp86 which is partially exposed to solvent at pH 8 + 4 M urea and further exposed at pH 2 + 4 M urea but apparently still in a highly asymmetrical environment (represented by *; see Figure 4C). The solid circle next to the W represents the degree of quenching of Trp86 intrinsic fluorescence with the largest quenching occurring at pH 8 ± 4 M urea (see Figure 4A).

pH have large effects on the mode and strength of self-association. Native pGH at pH 8 undergoes a weak but discrete self-association where the largest species appears to be the tetramer, while the presence of 4 M urea at pH 8 almost eliminates self-association, presumably by altering the interactive surface landscape (*51*, *52*). Note that the I_{340} for Trp86 at pH 8 in the presence of urea is ~25% larger than in the absence of urea (Figure 1A) and that λ_{max} is red shifted by >5 nm (Figure 1B). This indicates that Trp86 is more exposed to solvent in the presence of urea than in its absence at pH 8. The effect of urea on self-association is unlikely to result from a covolume or "crowding" effect since this would normally enhance self-association (*53*).

At pH 2 ± urea, pGH intermediates undergo strong monomer−dimer self-association to the point where monomer cannot be detected over the protein concentration range observed. The value of K for this dimerization is $\geq \sim 5 \times 10^6$ M^{-1}. We speculate that this dimer is an off-pathway folding intermediate. It is capable of further reversible self-association described by values of K at least 1 order of magnitude smaller than that for the formation of the dimer (Table 2). In the absence of urea, the self-association proceeds by unlimited addition of dimers which we represent as occurring in a classical "head-to-tail" fashion (Figure 8).

The presence of 4 M urea at pH 2 does not measurably affect the strong formation of dimer, and this infers that this concentration of urea does not alter the binding sites responsible for this interaction. However, head-to-tail self-association is replaced by a discrete self-association where the largest species appears to be the octamer. This implies that the presence of urea at pH 2 acts to remove some binding sites from the surface of pGH and create new self-association sites. One of these new binding sites may involve the residues found in helix 3 of the native protein's four-helix bundle. The addition of a helix 3-containing peptide to a Gdn-HCl-induced folding intermediate of bGH reduces its polymerization (*54*). Furthermore, this reduction correlates with a loss of a prominent θ_{300} peak (*54*), a peak we also observe for pGH at pH 2 + 4 M urea.

Thus, the critical off-pathway folding intermediate for pGH (and probably bGH) may be the highly favorable formation of a dimer. The mode of self-association of this dimer then depends on its exact conformation. Certain conformations of the dimerized intermediate (e.g., at pH 2 + 4 M urea) undergo further discrete self-association, which may involve helix 3 residues and which correlates with changes in θ_{300}. Other conformations of the off-pathway dimer undergo more extensive self-association, which does not correlate with changes in θ_{300} and which may not involve helix 3 residues (e.g., at pH 2 minus urea). We are currently undertaking experiments to test this. pGH thus provides further evidence that, within a family of proteins, folding intermediates can display a great range of structural variability and ability to polymerize.

REFERENCES

1. Kim, P. S., and Baldwin, R. L. (1982) *Annu. Rev. Biochem. 51*, 459−489.
2. Kim, P. S., and Baldwin, R. L. (1990) *Annu. Rev. Biochem. 59*, 631−660.
3. Ptitsyn, O. B. (1995) *Adv. Protein Chem. 47*, 83−229.
4. Kuwajima, K. (1989) *Proteins: Struct., Funct., Genet. 6*, 87−103
5. Dobson, C. M. (1994) *Curr. Biol. 4*, 636−640.
6. Ptitsyn, O. B. (1992) in *Protein Folding* (Creighton, T. E., Ed.) pp 243−300, W. H. Freeman & Co., New York.
7. Hayer-Hartl, M. K., Ewbank, J. J., Creighton, T. E., and Hartl, F. U. (1994) *EMBO J. 13*, 3192−3202.
8. Thomas, P. J., Qu, B. H., and Pederson, P. L. (1995) *Trends Biol. Sci. 20*, 456−459.
9. Booth, D. R., Sunde, M., Bellotti, V., Robinson, C. V., Hutchinson, W. L., Fraser, P. E., Hawkins, P. N., Dobson, C. M., Radford, S. E., Blake, C. C. F., and Pepys, M. (1997) *Nature 385*, 787−793.
10. Goto, Y., Calciano, L. J., and Fink, A. L. (1990) *Proc. Natl. Acad. Sci. U.S.A. 87*, 573−577.
11. Goto, Y., Takahashi, N., and Fink, A. L. (1990) *Biochemistry 29*, 3480−3488.
12. Fink, A. L., Calciano, L. J., Goto, Y., Kurotsu, T., and Palleros, D. R. (1994) *Biochemistry 33*, 12504−12511.
13. Fink, A. L. (1995) *Annu. Rev. Biophys. Biomol. Struct. 24*, 495−522.

14. De Filippis, V., de Laureto, P. P., Toniutti, N., and Fontana, A. (1996) *Biochemistry 35*, 11503−11511.
15. Abdel-Meguid, S. S., Shieh, H.-S., Smith, W. W., Dayringer, H. E., Violand, B. N., and Bentle, L. A. (1987) *Proc. Natl. Acad. Sci. U.S.A. 84*, 6434−6437.
16. de Vos, A. M., Ultsch, M., and Kossiakoff, A. A. (1992) *Science 255*, 306−312.
17. Carlacci, L., Chou, K.-C., and Maggiora, G. M. (1991) *Biochemistry 30*, 4389−4398.
18. Kauffman, E. W., Thamann, T. J., and Havel, H. A. (1989) *J. Am. Chem. Soc. 111*, 5449−5456.
19. Holzman, T. F., Dougherty, J. J., Brems, D. N., and MacKenzie, N. E. (1990) *Biochemistry 29*, 1255−1261.
20. De Felippis, M. R., Kilcomons, M. A., Lents, M. P., Youngman, K. M., and Havel, H. A. (1995) *Biochim. Biophys. Acta 1247*, 35−45.
21. Bastiras, S., and Wallace, J. C. (1992) *Biochemistry 31*, 9304−9309.
22. Bailey, J. E., and Ollis, D. F. (1986) in *Biochemical Engineering Fundamentals*, 2nd ed., pp 403−404, MacGraw-Hill, New York.
23. Savitsky, A., and Golay, M. J. E. (1964) *Anal. Chem. 8*, 1627−1639.
24. Corbett, R. J. T., and Roche, R. S. (1984) *Biochemistry 23*, 1888−1894.
25. Teller, D. C. (1973) *Methods Enzymol. 27*, 346−441.
26. Milthorpe, B. K., Jeffrey, P. D., and Nichol, L. W. (1975) *Biophys. Chem. 3*, 169−176.
27. Cohn, E. J., and Edsall, J. T. (1943) *Proteins, Amino Acids and Peptides as Ions and Dipolar Ions*, Reinhold, New York.
28. Ralston, G. B., and Morris, M. B. (1992) in *Analytical Ultracentrifugation in Biochemistry and Polymer Science* (Harding, S. E., Rowe, A. J., and Horton, J. C., Eds.) pp 90−125, The Royal Society of Chemistry, Cambridge.
29. Adams, E. T., Tang, L.-H., Sarquis, J. L., Barlow, G. H., and Norman, W. M. (1978) in *Physical Aspects of Protein Interactions* (Catsimpoolas, N., Ed.) pp 1−55, Elsevier/North-Holland, Amsterdam.
30. Adams, E. T., and Fujita, H. (1963) in *Ultracentrifugal Analysis in Theory and Experiment* (Williams, J. W., Ed.) pp 119−129, Academic Press, New York.
31. Morris, M. B., and Ralston, G. B. (1985) *Biophys. Chem. 23*, 49−61.
32. Cleland, W. W. (1967) *Adv. Enzymol. Relat. Areas Mol. Biol. 21*, 1−32.
33. Pace, C. N. (1986) *Methods Enzymol. 131*, 266−280.
34. Havel, H. A. (1996) in *Spectroscopic Methods for Determining Protein Structure in Solution* (Havel, H. A., Ed.) pp 62−68, VCH Publishers, Inc., New York.
35. Bewley, T. A., and Li, C. H. (1984) *Arch. Biochem. Biophys. 233*, 219−227.
36. Havel, H. A., Kauffman, E. W., Plaisted, S. M., and Brems, D. N. (1986) *Biochemistry 25*, 6533−6538.
37. Bastiras, S. (1992) Ph.D. Thesis, Department of Biochemistry, University of Adelaide, South Australia.
38. Brems, D. N., Plaisted, S. M., Havel, H. A., Kauffman, E. W., Stodola, J. D., Eaton, L. C., and White, R. D. (1985) *Biochemistry 24*, 7662−7668.
39. Tanford, C. (1961) *Physical Chemistry of Macromolecules*, Wiley, New York.
40. Ribela, M. T. C. P., and Bartolini, P. (1988) *Anal. Biochem. 174*, 693−697.
41. Johnson, M. L., and Yphantis, D. A. (1978) *Biochemistry 17*, 1448−1455.
42. Rowlinson, S. W., Barnard, R., Bastiras, S., Robins, A. J., Senn, C., Wells, J. R., Brinkworth, R., and Waters, M. J. (1994) *Biochemistry 33*, 11724−11733.
43. Brems, D. N., Brown, P. L., and Becker, G. W. (1990) *J. Biol. Chem. 265*, 5504−5511.
44. Burger, H. G., Edelhoch, H., and Condliffe, P. G. (1966) *Endocrinology 78*, 98−102.
45. Donovan, J. W. (1973) *Methods Enzymol. 27*, 525−548.
46. Edelhoch, H., and Burger, H. G. (1966) *J. Biol. Chem. 241*, 458−63.
47. Geierstanger, B., Jamin, M., Volkman, B. F., and Baldwin, R. L. (1998) *Biochemistry 37*, 4254−4265.
48. MacKenzie, N. E., Plaisted, S. M., and Brems, D. N. (1989) *Biochim. Biophys. Acta 994*, 166−171.
49. DeFelippis, M. R., Alter, L. A., Pekar, A. H., Havel, H. A., and Brems, D. N. (1993) *Biochemistry 32*, 1555−1562.
50. Brems, D. N., Plaisted, S. M., Havel, H. A., and Tomich, C.-S. C. (1988) *Proc. Natl. Acad. Sci. U.S.A. 85*, 3367−3371.
51. Laskowski, R. A., Luscombe, N. M., Swindells, M. B., and Thornton, J. M. (1996) *Protein Sci. 5*, 2438−2452.
52. Young, L., Jernigan, R. L., and Covell, D. G. (1994) *Protein Sci. 3*, 717−729.
53. Shearwin, K. E., and Winzor, D. J. (1988) *Biophys. Chem. 31*, 287−294.
54. Brems, D. N., Plaisted, S. M., Kauffman, E. W., and Havel, H. A. (1986) *Biochemistry 25*, 6539−6543.

BI0005658